Topological Magnon-Phonon Hybrid Excitations in Two-Dimensional Ferromagnets with Tunable Chern Numbers

Gyungchoon Go,[1] Se Kwon Kim,[2,*] and Kyung-Jin Lee[1,3,†]
[1]Department of Materials Science and Engineering, Korea University, Seoul 02841, Korea
[2]Department of Physics and Astronomy, University of Missouri, Columbia, Missouri 65211, USA
[3]KU-KIST Graduate School of Converging Science and Technology, Korea University, Seoul 02841, Korea

(Received 4 July 2019; revised manuscript received 15 October 2019; published 5 December 2019)

We theoretically investigate magnon-phonon hybrid excitations in two-dimensional ferromagnets. The bulk bands of hybrid excitations, which are referred to as magnon polarons, are analytically shown to be topologically nontrivial, possessing finite Chern numbers. We also show that the Chern numbers of magnon-polaron bands and the number of band-crossing lines can be manipulated by an effective magnetic field. For experiments, we propose to use the thermal Hall conductivity as a probe of the finite Berry curvatures of magnon-polarons. Our results show that a simple ferromagnet on a square lattice supports topologically nontrivial magnon polarons, generalizing topological excitations in conventional magnetic systems.

DOI: 10.1103/PhysRevLett.123.237207

Introduction.—Since Haldane's prediction of the quantized Hall effect without Landau levels [1], intrinsic topological properties of electronic bands have emerged as a central theme in condensed matter physics. The band topology can be characterized by an emergent vector potential and associated magnetic field defined in momentum space for electron wave functions, called the Berry phase and Berry curvature, respectively [2]. The Berry curvature is responsible for various phenomena on electron transport such as the anomalous Hall effect [3,4] and the spin Hall effect [5–7]. In addition, nontrivial topology of bulk bands gives rise to chiral or helical edge states according to the bulk-boundary correspondence [8].

Recently, research on the effects of Berry curvature on transport properties, which was initiated for electron systems originally, has expanded to transport of collective excitations in various systems. In particular, magnetic insulators, which gather great attention in spintronics due to their utility for Joule-heat-free devices [9], have been investigated for nontrivial Berry phase effects on their collective excitations [10–26]: spin waves (magnons) and lattice vibrations (phonons). Previous studies exclusively considering either only magnons or only phonons showed that they can have the topological bands of their own, thereby exhibiting either the magnon Hall effect in chiral magnetic systems [10–25] or the phonon Hall effect [26] when the Raman spin-phonon coupling is present.

Interestingly, the hybridized excitation of magnons and phonons, called a magnetoelastic wave [27] or magnon polaron [28], is able to exhibit the Berry curvature and thus nontrivial topology due to magnon-phonon interaction [29–31], even though each of the magnon system and the phonon system has a trivial topology. In noncollinear antiferromagnets, the strain-induced change (called striction) of the exchange interaction is able to generate the nontrivial topology in the magnon-phonon hybrid system [29]. In ferromagnets, which are of the main focus in this work, nontrivial topology of magnon polarons is obtained by accounting for long-range dipolar interaction [30]. In addition, in ferromagnets with broken mirror symmetry, the striction of Dzyaloshinskii-Moriya (DM) interaction leads to topological magnon-polaron bands [31].

In this Letter, we theoretically investigate the topological aspects of the magnon-phonon hybrid excitation in a simple two-dimensional (2D) square-lattice ferromagnet with perpendicular magnetic anisotropy [see Fig. 1(a) for the illustration of the system]. Several distinguishing features of our model are as follows. Our model is optimized for atomically thin magnetic crystals, i.e., 2D magnets. The recent discovery of magnetism in 2D van der Waals materials opens huge opportunities for investigating unexplored rich physics and future spintronic devices in reduced dimensions [32–42]. Because we consider the 2D model, we ignore the nonlocal dipolar interaction, which is not a precondition for a finite Berry curvature in 2D magnets. Moreover, the Berry curvature we find does not require a special spin asymmetry such as the DM interaction nor a special lattice symmetry: Our 2D model description is applicable for general thin film ferromagnets. Therefore, we show in this work that even without such long-range dipolar interaction, DM interaction, or special lattice symmetry, the nontrivial topology of a magnon-phonon hybrid can emerge by taking account of the well-known magnetoelastic interaction driven by Kittel [43,44]. As Kittel's magnetoelastic interaction originates from the magnetic anisotropy, which is ubiquitous in ferromagnetic

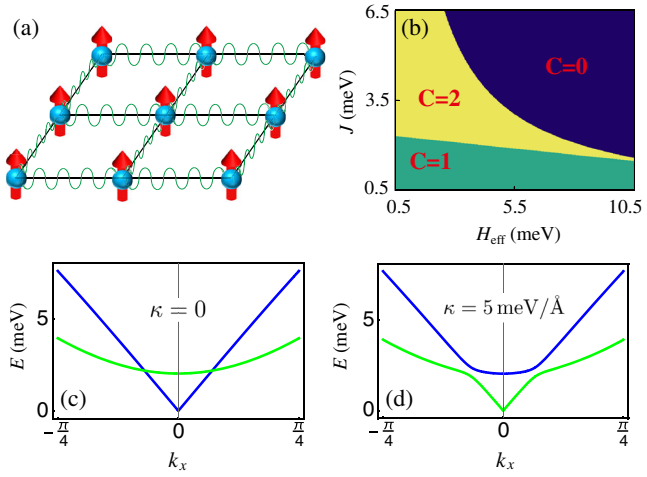

FIG. 1. (a) The schematic illustration of the magnon and phonon system. The ground state of the magnetization is given by the uniform spin state along the z axis (red arrow). (b) The Chern number of our magnon-phonon hybrid system. $H_{\rm eff}$ represents the effective magnetic field including the anisotropy field and the external magnetic field, $H_{\rm eff} = K_z S + \mathcal{B}$. (c), (d) Band dispersions without an external magnetic field $\mathcal{B}$. The used parameter values are given in the main text.

thin film structures [45], our result does not rely on specific preconditions but is quite generic. Furthermore, we show that the topological structures of the magnon-polaron bands can be manipulated by effective magnetic fields via topological phase transition. We uncover the origin of the nontrivial topological bands by mapping our model to the well-known two-band model for topological insulators [7], where the Chern numbers are read by counting the number of topological textures, called skyrmions, of a certain vector in momentum space. At the end of this Letter, we propose the thermal Hall conductivity as an experimental probe for our theory.

Model.—Our model system is a 2D ferromagnet on a square lattice described by the Hamiltonian

$$H = H_{\rm mag} + H_{\rm ph} + H_{\rm mp}, \tag{1}$$

where the magnetic Hamiltonian is given by

$$H_{\rm mag} = -J\sum_{\langle i,j\rangle} \mathbf{S}_i \cdot \mathbf{S}_j - \frac{K_z}{2}\sum_i S_{i,z}^2 - \mathcal{B}\sum_i S_{i,z}, \tag{2}$$

where $J > 0$ is the ferromagnetic Heisenberg exchange interaction, $K_z > 0$ is the perpendicular easy-axis anisotropy, and $\mathcal{B}$ is the external magnetic field applied along the easy axis. Throughout the Letter, we focus on the case where a ground state is the uniform spin state along the z axis: $\mathbf{S}_i = \hat{\mathbf{z}}$. The phonon system accounting for the elastic degree of freedom of the lattice is described by the following Hamiltonian:

$$H_{\rm ph} = \sum_i \frac{\mathbf{p}_i^2}{2M} + \frac{1}{2}\sum_{i,j,\alpha,\beta} u_i^\alpha \Phi_{i,j}^{\alpha,\beta} u_j^\beta, \tag{3}$$

where $\mathbf{u}_i$ is the displacement vector of the ith ion from its equilibrium position, $\mathbf{p}_i$ is the conjugate momentum vector, M is the ion mass, and $\Phi_{i,j}^{\alpha,\beta}$ is a force constant matrix. The magnetoelastic coupling is modeled by the following Hamiltonian term [43,44,46]:

$$H_{\rm mp} = \kappa \sum_i \sum_{\mathbf{e}} (\mathbf{S}_i \cdot \mathbf{e})(u_i^z - u_{i+\mathbf{e}}^z), \tag{4}$$

where κ is the strength of the magnon-phonon interaction and $\mathbf{e}$'s are the nearest neighbor vectors. Equation (4) describes the magnetoelastic coupling as a leading order in the magnon amplitude, where the in-plane components of the displacement vector do not appear (see Supplemental Material [47] for derivation).

We note here that our model Hamiltonian does not include the dipolar interaction and the DM interaction, distinct from the model considered in Refs. [30] and [31]. Because the above-mentioned interactions are absent in our model, neither the ferromagnetic system nor elastic system exhibits the thermal Hall effect when they are not coupled. In other words, they are invariant under the combined action of time reversal ($\mathcal{T}$) and spin rotation by 180° around an in-plane axis ($\mathcal{C}$) [31]. It is the magnetoelastic coupling term $H_{\rm mp}$ that breaks the combined symmetry $\mathcal{TC}$ and thus can give rise to the thermal Hall effect as will be shown below.

Magnon-phonon hybrid excitations.—We first diagonalize the magnetic Hamiltonian $H_{\rm mag}$ and the phonon Hamiltonian $H_{\rm ph}$ separately, and then obtain the magnon-phonon hybrid excitations, which are called magnon polarons, by taking account of the coupling term $H_{\rm mp}$.

The magnetic Hamiltonian is solved by performing the Holstein-Primakoff transformation $S_i^x \approx (\sqrt{2S}/2)(a_i + a_i^\dagger)$, $S_i^y \approx (\sqrt{2S}/2i)(a_i - a_i^\dagger)$, $S_i^z = S - a_i^\dagger a_i$, where a_i and $a_i^\dagger$ are the annihilation and the creation operators of a magnon at site i. By taking the Fourier transformation, $a_i = \sum_{\mathbf{k}} e^{i\mathbf{k}\cdot\mathbf{R}_i} a_{\mathbf{k}}/\sqrt{N}$, where N is the number of sites in the system, we diagonalize the magnetic Hamiltonian in the momentum space:

$$H_{\rm mag} = \sum_{\mathbf{k}} \hbar\omega_m(\mathbf{k}) a_{\mathbf{k}}^\dagger a_{\mathbf{k}}, \tag{5}$$

where the magnon dispersion is given by $\omega_m(\mathbf{k}) = [2JS(2 - \cos k_x - \cos k_y) + K_z S + \mathcal{B}]/\hbar$.

For the elastic Hamiltonian $H_{\rm ph}$, it is also convenient to describe in the momentum space:

$$H_{\rm ph} = \sum_{\mathbf{k}} \left(\frac{p^z_{-\mathbf{k}} p^z_{\mathbf{k}}}{2M} + \frac{1}{2} u^z_{-\mathbf{k}} \Phi(\mathbf{k}) u^z_{\mathbf{k}} \right), \tag{6}$$

where only nearest-neighbor elastic interactions are maintained as dominant terms and the momentum-dependent spring constant is $\Phi(\mathbf{k}) = M\omega_0^2(4 - 2\cos k_x - 2\cos k_y)$, where the characteristic vibration frequency ω_0 corresponds to the elastic interaction between two nearest-neighbor ions. To obtain the quantized excitations of the phonon system, we introduce the phonon annihilation operator $b_{\mathbf{k}}$ and the creation operator $b^\dagger_{\mathbf{k}}$ in such a way that

$$u^z_{\mathbf{k}} = \sqrt{\frac{\hbar}{M\omega_p(\mathbf{k})}} \left(\frac{b_{\mathbf{k}} + b^\dagger_{-\mathbf{k}}}{\sqrt{2}} \right), \tag{7}$$

$$p^z_{\mathbf{k}} = \sqrt{\hbar M \omega_p(\mathbf{k})} \left(\frac{b_{-\mathbf{k}} - b^\dagger_{\mathbf{k}}}{\sqrt{2}i} \right), \tag{8}$$

where the phonon dispersion is given by $\omega_p(\mathbf{k}) = \omega_0\sqrt{4 - 2\cos k_x - 2\cos k_y}$. This leads to the following diagonalized phonon Hamiltonian:

$$H_{\rm ph} = \sum_{\mathbf{k}} \hbar\omega_p(\mathbf{k}) \left(b^\dagger_{\mathbf{k}} b_{\mathbf{k}} + \frac{1}{2} \right). \tag{9}$$

In terms of the magnon and phonon operators introduced above, the magnetoelastic coupling term is recast into the following form in the momentum space: $H_{\rm mp} = H_{\rm mp1} + H_{\rm mp2}$, where

$$H_{\rm mp1} = \tilde{\kappa} \sum_{\mathbf{k}} [a^\dagger_{\mathbf{k}} b_{\mathbf{k}} (-i \sin k_x + \sin k_y)] + \text{H.c.}, \tag{10}$$

$$H_{\rm mp2} = \tilde{\kappa} \sum_{\mathbf{k}} [a^\dagger_{-\mathbf{k}} b^\dagger_{\mathbf{k}} (i \sin k_x - \sin k_y)] + \text{H.c.}, \tag{11}$$

with $\tilde{\kappa} = \kappa\sqrt{\hbar S/[M\omega_p(\mathbf{k})]}$. Note that $H_{\rm mp1}$ conserves the total particle number, whereas $H_{\rm mp2}$ does not. Because of $H_{\rm mp2}$, the total Hamiltonian takes the Bogoliubov–de-Gennes (BdG) form.

The band structure of the magnon-phonon hybrid system is obtained by solving the Heisenberg equations with the above results [Eqs. (1)–(10)] (see the Supplemental Material [47] for the detailed calculation and the schematic illustration of the band structure [47]). Without magnon-phonon interaction, there are two positive branches consisting of a magnon band and a phonon band. The two bands cross at $\mathbf{k}$ points satisfying $\omega_m(\mathbf{k}) = \omega_p(\mathbf{k})$ [see Fig. 1(c)]. Different from the conventional Dirac system, there are innumerable band-crossing points which form a closed line. These band-crossing lines are removed by the magnon-phonon interaction $\propto \kappa$ [see Fig. 1(d)], which induces the nontrivial topological property of the bands, characterized by the Berry curvatures. In the BdG Hamiltonian, the Berry curvature is given by [19,29,31]

$$\mathbf{\Omega}_n(\mathbf{k}) = \nabla \times \mathbf{A}_n(\mathbf{k}), \tag{12}$$

where $\mathbf{A}_n = i\langle\psi_{n,\mathbf{k}}|\mathcal{J}\nabla_{\mathbf{k}}|\psi_{n,\mathbf{k}}\rangle$ and $\psi_{n,\mathbf{k}}$ are the nth eigenstates (see Supplemental Material [47] for details). The topological property of the whole system is determined by the Chern number of bands, which is the integral of the Berry curvature over the Brillouin zone [48]. In Fig. 1(b), we show the Chern number of our bosonic system with nonzero magnon-phonon interaction κ. In our system, the Chern number can be one of three integers (0, 1, and 2) depending on the effective magnetic field $H_{\rm eff} = K_z S + \mathcal{B}$ and exchange interaction J. This is one of our central results: The magnon-polaron bands in a 2D simple square-lattice ferromagnet are topologically nontrivial even in the absence of dipolar or DM interaction and their topological property can be controlled by the effective magnetic field.

Origin of the topological property.—The origin of the nontrivial magnon-polaron bands obtained above can be understood through the mapping of our system to the well-known model for two-dimensional topological insulators such as HgTe [7,48]. Considering $H_{\rm mp}$ as a weak perturbation with unperturbed Hamiltonian with well-defined energies of magnons and phonons, the effect of the particle-number-nonconserving component $H_{\rm mp2}$ on the band structure is much smaller than that of particle-number-conserving part $H_{\rm mp1}$. Neglecting $H_{\rm mp2}$, the total Hamiltonian is simplified into a single-particle two-band Hamiltonian

$$H \approx \sum_{\mathbf{k}} \begin{pmatrix} a^\dagger_{\mathbf{k}} & b^\dagger_{\mathbf{k}} \end{pmatrix} \mathcal{H}_{\mathbf{k}} \begin{pmatrix} a_{\mathbf{k}} \\ b_{\mathbf{k}} \end{pmatrix}, \tag{13}$$

where

$$\mathcal{H}_{\mathbf{k}} = \begin{pmatrix} \hbar\omega_m(\mathbf{k}) & \tilde{\kappa}(\sin k_y - i \sin k_x) \\ \tilde{\kappa}(\sin k_y + i \sin k_x) & \hbar\omega_p(\mathbf{k}) \end{pmatrix}. \tag{14}$$

In terms of the Pauli matrices $\boldsymbol{\sigma} = (\sigma_x, \sigma_y, \sigma_z)$, we write Eq. (14) in a more compact form

$$\mathcal{H}_{\mathbf{k}} = \frac{\hbar}{2}[\omega_m(\mathbf{k}) + \omega_p(\mathbf{k})] I_{2\times 2} + \mathbf{d}(\mathbf{k}) \cdot \boldsymbol{\sigma}, \tag{15}$$

where

$$\mathbf{d}(\mathbf{k}) = \left(\tilde{\kappa} \sin k_y, \tilde{\kappa} \sin k_x, \frac{\hbar}{2}[\omega_m(\mathbf{k}) - \omega_p(\mathbf{k})] \right). \tag{16}$$

The band structure for the above Hamiltonian is given by

$$E_\pm(\mathbf{k}) = \frac{\hbar}{2}[\omega_m(\mathbf{k}) + \omega_p(\mathbf{k})] \pm |\mathbf{d}(\mathbf{k})|. \tag{17}$$

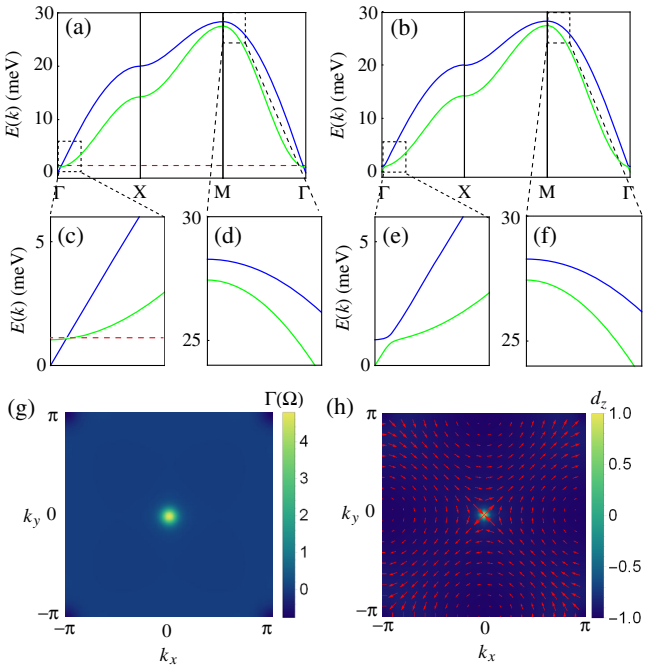

FIG. 2. The band structure and its topology for the $|C| = 1$ case. The band structure for $\kappa = 0$ (a),(c),(d) and $\kappa = 5$ meV/Å (b),(e),(f). The red-dashed line represents the band-crossing points. (g) Berry curvatures of the upper band in log scale $\Gamma(\Omega^z) = \mathrm{sgn}(\Omega^z)\log(1 + |\Omega^z|)$ for $\kappa = 5$ meV/Å (h) Schematic illustration of $\hat{\mathbf{d}}(\mathbf{k})$ for $\kappa = 5$ meV/Å. The in-plane components $(\hat{d}_x, \hat{d}_y)$ are shown in red arrows.

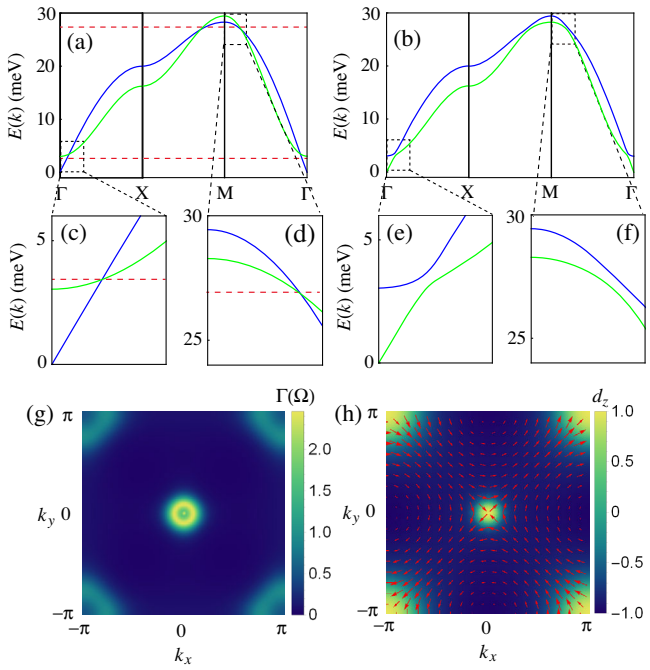

FIG. 3. The band structure and its topology for the $|C| = 2$ case. The band structure for $\kappa = 0$ (a),(c),(d) and $\kappa = 5$ meV/Å (b),(e),(f). The red dashed lines represent the band-crossing points. (g) Berry curvatures of the upper band in log scale $\Gamma(\Omega^z) = \mathrm{sgn}(\Omega^z)\log(1 + |\Omega^z|)$ for $\kappa = 5$ meV/Å. (h) Schematic illustration of $\hat{\mathbf{d}}(\mathbf{k})$ for $\kappa = 5$ meV/Å. The in-plane components $(\hat{d}_x, \hat{d}_y)$ are shown in red arrows.

In terms of $\mathbf{d}$ vectors, the Berry curvature is written explicitly as

$$\Omega^z_{\pm}(\mathbf{k}) = \mp\frac{1}{2}\hat{\mathbf{d}}(\mathbf{k}) \cdot \left(\frac{\partial\hat{\mathbf{d}}(\mathbf{k})}{\partial k_x} \times \frac{\partial\hat{\mathbf{d}}(\mathbf{k})}{\partial k_y}\right). \tag{18}$$

The corresponding expression for the Chern number is given by [48–50]

$$C_{\pm} = \frac{1}{2\pi}\int dk_x dk_y \Omega^z_{\pm}(\mathbf{k}), \tag{19}$$

which is the skyrmion number of the $\mathbf{d}$ vector [48], counting how many times $\hat{\mathbf{d}}$ wraps the unit sphere in the Brillouin zone. From Eq. (14), we read that the magnon band and phonon band cross at $\mathbf{k}$ points satisfying $\omega_m(\mathbf{k}) = \omega_p(\mathbf{k})$ without the magnon-phonon interaction. These band crossing points are opened by the magnon-phonon interaction $\propto \kappa$ and the finite Berry curvatures are induced near the gap opening region. After integrating the Berry curvatures over the Brillouin zone, we obtain $C_{\pm} = 0$, ± 1, or ± 2. The two-band model has almost identical band structures and Berry curvatures to those of full Hamiltonian, where H_{mp2} is additionally considered (see the Supplemental Material [47]).

In Figs. 2 and 3, we show that the bulk band structures and their topological properties for $|C| = 1$ and $|C| = 2$, respectively. For calculation, we use the parameters of the monolayer ferromagnet CrI_3 in Refs. [31,33,36,51] ($J = 2.2$ meV, $K_z = 1.36$ meV, $S = 3/2$, and $Mc^2 = 5 \times 10^{10}$ eV). The force constant between the nearest-neighbor phonon is assumed as $\hbar\omega_0 = 10$ meV. We use $\kappa = 5$ meV/ Å and a lattice constant $a = 5$ Å, yielding $\kappa S^2/a^2 \approx 7.2 \times 10^7$ J/m^3, which is comparable in magnitude with magnetoelastic constant in a Co film [52]. The external magnetic field $\mathcal{B} = -1$ meV is chosen for Fig. 2 and $\mathcal{B} = 1$ meV is chosen for Fig. 3. In Figs. 2(a) and 2(c), we find a band-crossing line (red dashed line), which is removed by the magnon-phonon interaction [Figs. 2(b) and 2(e)]. In this case, a dominant contribution of the Berry curvature comes from the vicinity of the Γ point [Fig. 2(g)]. An intuitive way to verify the topological nature of the system is the number of skyrmions of the unit vector $\hat{\mathbf{d}}(\mathbf{k})$. In Fig. 2(h), we find that there is a skyrmion at the Γ-point corresponding to $|C| = 1$. By changing the sign of the external magnetic field $\mathcal{B}$, we can modify the band structure with two band-crossing lines [Figs. 3(a), 3(c), and 3(d)]. In this case, the dominant contribution of the Berry curvature comes from vicinity of the Γ and M points [Fig. 3(g)]. In terms of $\hat{\mathbf{d}}(\mathbf{k})$, we find that one skyrmion is located at the Γ

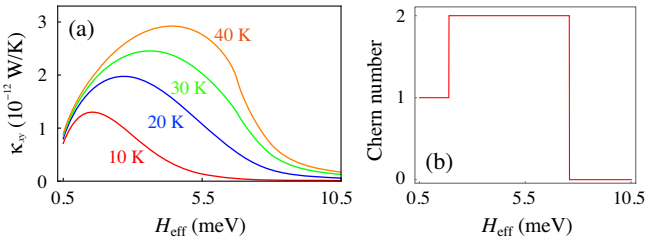

FIG. 4. (a) Dependence of thermal Hall conductivity on the effective magnetic field $H_{\rm eff}$ and with different temperatures T using the parameters in the main text. (b) Dependence of Chern number on the effective magnetic field $H_{\rm eff}$ using the parameters in the main text.

point and the other skyrmion is at the M point corresponding to $|C| = 2$ [Fig. 3(h)]. We note that the magnetic atoms in CrI_3 form a honeycomb lattice, differing from a square lattice considered here. However, regardless of the lattice structure, our description based on a square lattice is still valid on Γ-point physics, which is characterized by long-wavelength excitations. The M-point physics in the honeycomb lattice structure would be different from our model.

Thermal Hall effect.—The finite Berry curvatures of magnon-phonon hybrid excitations give rise to the intrinsic thermal Hall effect as shown below. The semiclassical equations of motion for the wave packet of the magnon-phonon hybrid are given by [2,53]

$$\dot{\mathbf{r}}_n = \frac{1}{\hbar}\frac{\partial E_n(\mathbf{k})}{\partial \mathbf{k}} - \dot{\mathbf{k}} \times \mathbf{\Omega}_n(\mathbf{k}), \qquad \hbar\dot{\mathbf{k}} = -\nabla U(\mathbf{r}), \tag{20}$$

where $U(\mathbf{r})$ is the potential acting on the wave packet, which can be regarded as a confining potential of the bosonic excitation. Near the edge of the sample, the gradient of the confining potential produces the anomalous velocity, $\nabla U(\mathbf{r}) \times \mathbf{\Omega}_n(\mathbf{k})$. In equilibrium, the edge current circulates along the whole edge and the net magnon current is zero along any in-plane direction. However, if the temperature varies spatially, the circulating current does not cancel, which causes the thermal Hall effect [12].

The Berry-curvature-induced thermal Hall conductivity is given by [12,13]

$$\kappa^{xy} = -\frac{k_B^2 T}{\hbar V}\sum_{n,\mathbf{k}} c_2(\rho_{n,\mathbf{k}})\Omega_n^z(\mathbf{k}), \tag{21}$$

where $c_2(\rho) = (1+\rho)\ln^2[(1+\rho)/\rho] - \ln^2\rho - 2\mathrm{Li}_2(-\rho)$, $\rho_{n,\mathbf{k}} = [e^{[E_n(\mathbf{k})]/k_B T - 1}]^{-1}$ is the Bose-Einstein distribution function with a zero chemical potential, k_B is the Boltzmann constant, T is the temperature, and $\mathrm{Li}_2(z)$ is the polylogarithm function. In Fig. 4(a), we show the dependence of thermal Hall conductivity on the effective magnetic field $H_{\rm eff}$ at different temperatures T. For small $H_{\rm eff}$, the thermal Hall conductivity increases with increasing $H_{\rm eff}$. However, for large $H_{\rm eff}$, it decreases with increasing $H_{\rm eff}$. This behavior of the thermal Hall conductivity can be understood through the Chern number of magnon-polaron bands depicted in Fig. 4(b). The absolute value of the Chern number is 1 for small $H_{\rm eff}$, then it jumps up to 2 for a certain value of $H_{\rm eff}$ and vanishes for large $H_{\rm eff}$.

Discussions.—In this Letter, we investigate the topology of the magnon-polaron bands in a simple 2D ferromagnet without long-range dipolar interaction and DM interaction. In our model, the topological structure can be controlled by the effective magnetic field which changes the number of band-crossing lines. Using a perturbation approach, we develop a two-band model Hamilitonian which provides an intuitive understanding of the topological structure of the model. In the two-band model, the nontrivial topology of the magnon-polaron bands are reflected in the skyrmion number of $\mathbf{d}(\mathbf{k})$ in momentum space. As an experimental demonstration, we propose that the thermal Hall conductivity arises from the nontrivial topology of the magnon-polaron bands. The thermal Hall conductivity depends on the effective magnetic field, which can be manipulated by the external magnetic field or voltage-induced magnetic anisotropy change [54]. Our results show that the magnetoelastic interaction generates nontrivial topology in simple 2D ferromagnets with topological tunability, suggesting the ubiquity of topological transports in conventional magnetic systems with reduced dimensions.

K.-J. L. acknowledges support by the National Research Foundation (NRF) of Korea (NRF-2017R1A2B2006119). G. G. acknowledges a support by the NRF of Korea (NRF-2019R1I1A1A01063594). S. K. K. was supported by the startup fund at the University of Missouri.

*kimsek@missouri.edu
†kj_lee@korea.ac.kr

[1] F. D. M. Haldane, Model for a Quantum Hall Effect without Landau Levels: Condensed-Matter Realization of the "Parity Anomaly", Phys. Rev. Lett. **61**, 2015 (1988).
[2] D. Xiao, M.-C. Chang, and Q. Niu, Berry phase effects on electronic properties, Rev. Mod. Phys. **82**, 1959 (2010).
[3] S. Onoda, N. Sugimoto, and N. Nagaosa, Intrinsic Versus Extrinsic Anomalous Hall Effect in Ferromagnets, Phys. Rev. Lett. **97**, 126602 (2006).
[4] N. A. Sinitsyn, A. H. MacDonald, T. Jungwirth, V. K. Dugaev, and J. Sinova, Anomalous Hall effect in a two-dimensional Dirac band: The link between the Kubo-Streda formula and the semiclassical Boltzmann equation approach, Phys. Rev. B **75**, 045315 (2007).
[5] S. Murakami, N. Nagaosa, and S.-C. Zhang, Dissipationless quantum spin current at room temperature, Science **301**, 1348 (2003).
[6] C. L. Kane and E. J. Mele, Z_2 Topological Order and the Quantum Spin Hall Effect, Phys. Rev. Lett. **95**, 146802 (2005).

[7] B. A. Bernevig, T. L. Hughes, and S.-C. Zhang, Quantum spin Hall effect and topological phase transition in HgTe quantum wells, Science **314**, 1757 (2006).

[8] Y. Hatsugai, Chern Number and Edge States in the Integer Quantum Hall Effect, Phys. Rev. Lett. **71**, 3697 (1993).

[9] Y. Kajiwara, K. Harii, S. Takahashi, J. Ohe, K. Uchida, M. Mizuguchi, H. Umezawa, H. Kawai, K. Ando, K. Takanashi, S. Maekawa, and E. Saitoh, Transmission of electrical signals by spin-wave interconversion in a magnetic insulator, Nature (London) **464**, 262 (2010).

[10] H. Katsura, N. Nagaosa, and P. A. Lee, Theory of the Thermal Hall Effect in Quantum Magnets, Phys. Rev. Lett. **104**, 066403 (2010).

[11] Y. Onose, T. Ideue, H. Katsura, Y. Shiomi, N. Nagaosa, and Y. Tokura, Observation of the magnon Hall effect, Science **329**, 297 (2010).

[12] R. Matsumoto and S. Murakami, Theoretical Prediction of a Rotating Magnon Wave Packet in Ferromagnets, Phys. Rev. Lett. **106**, 197202 (2011).

[13] R. Matsumoto and S. Murakami, Rotational motion of magnons and the thermal Hall effect, Phys. Rev. B **84**, 184406 (2011).

[14] R. Shindou, R. Matsumoto, S. Murakami, and J.-i. Ohe, Topological chiral magnonic edge mode in a magnonic crystal, Phys. Rev. B **87**, 174427 (2013).

[15] R. Shindou, J.-i. Ohe, R. Matsumoto, S. Murakami, and E. Saitoh, Chiral spin-wave edge modes in dipolar magnetic thin films, Phys. Rev. B **87**, 174402 (2013).

[16] L. Zhang, J. Ren, J.-S. Wang, and B. Li, Topological magnon insulator in insulating ferromagnet, Phys. Rev. B **87**, 144101 (2013).

[17] A. Mook, J. Henk, and I. Mertig, Edge states in topological magnon insulators, Phys. Rev. B **90**, 024412 (2014).

[18] S. K. Kim, H. Ochoa, R. Zarzuela, and Y. Tserkovnyak, Realization of the Haldane-Kane-Mele Model in a System of Localized Spins, Phys. Rev. Lett. **117**, 227201 (2016).

[19] R. Cheng, S. Okamoto, and D. Xiao, Spin Nernst Effect of Magnons in Collinear Antiferromagnets, Phys. Rev. Lett. **117**, 217202 (2016).

[20] S. A. Owerre, A first theoretical realization of honeycomb topological magnon insulator, J. Phys. Condens. Matter **28**, 386001 (2016).

[21] V. A. Zyuzin and A. A. Kovalev, Magnon Spin Nernst Effect in Antiferromagnets, Phys. Rev. Lett. **117**, 217203 (2016).

[22] K. Nakata, S. K. Kim, J. Klinovaja, and D. Loss, Magnonic topological insulators in antiferromagnets, Phys. Rev. B **96**, 224414 (2017).

[23] B. Göbel, A. Mook, J. Henk, and I. Mertig, Unconventional topological Hall effect in skyrmion crystals caused by the topology of the lattice, Phys. Rev. B **95**, 094413 (2017).

[24] S. K. Kim, K. Nakata, D. Loss, and Y. Tserkovnyak, Tunable Magnonic Thermal Hall Effect in Skyrmion Crystal Phases of Ferrimagnets, Phys. Rev. Lett. **122**, 057204 (2019).

[25] S. A. Díaz, J. Klinovaja, and D. Loss, Topological Magnons and Edge States in Antiferromagnetic Skyrmion Crystals, Phys. Rev. Lett. **122**, 187203 (2019).

[26] L. Zhang, J. Ren, J.-S. Wang, and B. Li, Topological Nature of the Phonon Hall Effect, Phys. Rev. Lett. **105**, 225901 (2010).

[27] N. Ogawa, W. Koshibae, A. J. Beekman, N. Nagaosa, M. Kubota, M. Kawasaki, and Y. Tokura, Photodrive of magnetic bubbles via magnetoelastic waves, Proc. Natl. Acad. Sci. U.S.A. **112**, 8977 (2015).

[28] T. Kikkawa, K. Shen, B. Flebus, R. A. Duine, K.-i. Uchida, Z. Qiu, G. E. W. Bauer, and E. Saitoh, Magnon polarons in the spin seebeck effect, Phys. Rev. Lett. **117**, 207203 (2016).

[29] S. Park and B.-J. Yang, Topological magnetoelastic excitations in noncollinear antiferromagnets, Phys. Rev. B **99**, 174435 (2019).

[30] R. Takahashi and N. Nagaosa, Berry Curvature in Magnon-Phonon Hybrid Systems, Phys. Rev. Lett. **117**, 217205 (2016).

[31] X. Zhang, Y. Zhang, S. Okamoto, and D. Xiao, Thermal Hall Effect Induced by Magnon-Phonon Interactions, Phys. Rev. Lett. **123**, 167202 (2019).

[32] M. A. McGuire, H. Dixit, V. R. Cooper, and B. C. Sales, Coupling of crystal structure and magnetism in the layered, ferromagnetic insulator CrI_3, Chem. Mater. **27**, 612 (2015).

[33] W.-B. Zhang, Q. Qu, P. Zhu, and C.-H. Lam, Robust intrinsic ferromagnetism and half semiconductivity in stable two-dimensional single-layer chromium trihalides, J. Mater. Chem. C **3**, 12457 (2015).

[34] J. U. Lee, S. Lee, J. H. Ryoo, S. Kang, T. Y. Kim, P. Kim, C.-H. Park, J.-G. Park, and H. Cheong, Ising-type magnetic ordering in atomically thin $FePS_3$, Nano Lett. **16**, 7433 (2016).

[35] C. Gong *et al.*, Discovery of intrinsic ferromagnetism in two-dimensional van der Waals crystals, Nature (London) **546**, 265 (2017).

[36] B. Huang *et al.*, Layer-dependent ferromagnetism in a van der Waals crystal down to the monolayer limit, Nature (London) **546**, 270 (2017).

[37] M. Bonilla, S. Kolekar, Y. Ma, H. C. Diaz, V. Kalappattil, R. Das, T. Eggers, H. R. Gutierrez, M.-H. Phan, and M. Batzill, Strong room-temperature ferromagnetism in VSe_2 monolayers on van der Waals substrates, Nat. Nanotechnol. **13**, 289 (2018).

[38] D. J. O'Hara *et al.*, Room temperature intrinsic ferromagnetism in epitaxial manganese selenide films in the monolayer limit, Nano Lett. **18**, 3125 (2018).

[39] Z. Fei *et al.*, Two-dimensional itinerant ferromagnetism in atomically thin Fe_3GeTe_2, Nat. Mater. **17**, 778 (2018).

[40] Y. Deng *et al.*, Gate-tunable room-temperature ferromagnetism in two-dimensional Fe_3GeTe_2, Nature (London) **563**, 94 (2018).

[41] K. S. Burch, D. Mandrus, and J.-G. Park, Magnetism in twodimensional van der Waals materials, Nature (London) **563**, 47 (2018).

[42] M. Gibertini, M. Koperski, A. F. Morpurgo, and K. S. Novoselov, Magnetic 2D materials and heterostructures, Nat. Nanotechnol. **14**, 408 (2019).

[43] C. Kittel, Physical, theory of ferromagnetic domains, Rev. Mod. Phys. **21**, 541 (1949).

[44] C. Kittel, Interaction of spin waves and ultrasonic waves in ferromagnetic crystals, Phys. Rev. **110**, 836 (1958).

[45] B. Dieny and M. Chshiev, Perpendicular magnetic anisotropy at transition metal/oxide interfaces and applications, Rev. Mod. Phys. **89**, 025008 (2017).

[46] E. Thingstad, A. Kamra, A. Brataas, and A. Sudbø, Chiral Phonon Transport Induced by Topological Magnons, Phys. Rev. Lett. **122**, 107201 (2019).

[47] See Supplemental Material at http://link.aps.org/supplemental/10.1103/PhysRevLett.123.237207 for detail calculations.

[48] X.-L. Qi, T. L. Hughes, and S.-C. Zhang, Topological field theory of time-reversal invariant insulators, Phys. Rev. B **78**, 195424 (2008).

[49] X.-L. Qi, Y.-S. Wu, and S.-C. Zhang, Topological quantization of the spin Hall effect in two-dimensional paramagnetic semiconductors, Phys. Rev. B **74**, 085308 (2006).

[50] G. E. Volovik, An analog of the quantum Hall effect in a superfluid ^{3}He film, Sov. Phys. JETP **67**, 1804 (1988).

[51] J. L. Lado and J. Fernández-Rossier, On the origin of magnetic anisotropy in two dimensional CrI_3, 2D Mater. **4**, 035002 (2017).

[52] Th. Gutjahr-Lösser, D. Sander, and J. Kirschner, Magnetoelastic coupling in Co thin films on W(0 0 1), J. Magn. Magn. Mater. **220**, L1 (2000).

[53] G. Sundaram and Q. Niu, Wave-packet dynamics in slowly perturbed crystals: Gradient corrections and Berry-phase effects, Phys. Rev. B **59**, 14915 (1999).

[54] T. Maruyama, Y. Shiota, T. Nozaki, K. Ohta, N. Toda, M. Mizuguchi, A. A. Tulapurkar, T. Shinjo, M. Shiraishi, S. Mizukami, Y. Ando, and Y. Suzuki, Large voltage-induced magnetic anisotropy change in a few atomic layers of iron, Nat. Nanotechnol. **4**, 158 (2009).